UNSTEADY FLOWS AROUND AN OSCILLATING FLAT PLATE MODEL USING AN EMBODIED TECHNIQUE OF FIBRE OPTICS LASER VELOCIMETER

D. Favier* , C. Maresca* and J. Belleudy**
Institut de Mécanique des Fluides, UM 34 du C.N.R.S.
1, Rue Honnorat 13003, Marseille-France

Abstract

The development of a new Laser Velocimetry technique suited for unsteady flow measurements near a moving surface is presented in this paper. The measurement method is based on an LV optical fibre option using an optical head embodied inside the moving model. Instantaneous velocity profiles and boundary-layer characteristics are obtained in a reference frame linked with the motion of the model. The unsteady acquisition and data reduction techniques are described and applied to the flow around a flat plate either at rest in the steady flow or oscillating in fore-and-aft motion. Details of the steady and unsteady boundary-layer measurements performed on the oscillating plate using the LV optical fibre technique are also compared to existing experimental and theoretical results obtained on a fixed model placed in oscillatory flow.

Nomenclature

A	=	amplitude displacement of the model in fore-and-aft motion, m
c	=	chord of the flat plate model, m
f	=	frequency of the oscillation , Hz
k	=	reduced frequency of oscillation, $c\omega/2U_\infty$
R_{ex}	=	local Reynolds number, $R_{ex} = U_\infty x/\nu$
R_{ec}	=	Reynolds number based on the model chord, $R_{ec} = U_\infty c/\nu$
t	=	time, sec
T	=	period of oscillation, $T = 1/f$
u	=	longitudinal boundary-layer velocity parallel to the wall, $m.s^{-1}$
Δu	=	amplitude of oscillating component of u, $m.s^{-1}$
U_e	=	local external velocity, $m.s^{-1}$
ΔU_e	=	amplitude of external velocity, $m.s^{-1}$
U_∞	=	freestream velocity, $m.s^{-1}$
x	=	distance parallel to the wall from the leading edge, m
$\overline{X}$	=	local dimenssionless frequency parameter, $\overline{X} = \omega x/U_\infty$
y	=	distance normal to the wall, m
α_0	=	incidence of the plate, deg
δ	=	boundary-layer thickness at 0.99 U_e, m
λ	=	reduced amplitude of oscillation, $\lambda = A\omega/U_\infty$
ν	=	kinematic viscosity, $m.s^{-1}$
ρ	=	air density, $Kg.m^{-3}$
Φ	=	phase angle of oscillating velocity relative to the freestream, deg
ω	=	angular frequency, $rad.s^{-1}$
ωt	=	phase of the oscillation, deg

* CNRS Senior Research Scientist. AIAA Member.
** IMFM Graduate Student.

I. Introduction

A better knowledge of the boundary-layer response to unsteadiness produced by a moving wall is of major interest in a wide variety of pratical aeronautical applications (see references 1 to 6). A few examples of the effects of unsteadiness on the boundary-layer behavior include changes in transition from laminar to turbulent location and the ensuing changes in turbulent separation location. Those unsteady changes affect the overall aerodynamic characteristics of the airfoil and can give rise to strong unsteady phenomena, such as bubble development, vortex formation and/or dynamic stall process.

Different numerical methods including 2D and 3D boundary-layer equations and full Navier-Stokes solvers are now available[7-12], as well as new experimental techniques for measurement of nonsteady local and/or overall aerodynamic quantities[13-19]. Among those experimental methods including different multiple hot-wires and hot-films techniques, the Laser Velocimetry[20-23] has contributed to comprehend the physical insights of basic unsteady flow configurations.

However, if boundary-layer measurements are quite easy to perform when the body is at rest in unsteady flow (pulsated flow for instance), the practice becomes more difficult when considering bodies performing time-dependent motions in the uniform freestream.

The purpose of this paper is to describe the advancement of a new Laser Velocimetry technique suited for unsteady boundary-layer measurements around moving walls. The measurement principle is based on an LV optical fibre system using an optical head embodied inside the moving model. Instantaneous boundary-layer velocity profiles are

thus obtained in a reference frame linked with the model oscillating in fore-and-aft motion and using appropriate acquisition and reduction data procedures described in the following sections.

II. Experimental Facilities and Measurement Procedures

The tests are conducted at IMF Marseille in the S3 subsonic wind-tunnel (rectangular test section : 0.5 x $1m^2$; length : 3 m), where the freestream velocity can be varied from 2.5 to 25 ms^{-1}, providing a Reynolds number range based on the model chord $5 \times 10^4 \leq Rec \leq 4 \times 10^5$. The test section turbulence level is less than 0.2%.

The experimental set up is shown in Fig. 1. The flat plate is supported in a vertical position and attached to the oscillating system by a single support shaft located at the quarter-chord axis of the model. Different kinds of oscillation of the model are allowed : fore-and-aft, plunging, pitching and coupled translation/pitch motion[18,19]. As shown in Fig. 2a, the leading-edge and trailing-edge consist respectively of an elliptical nose of 1/3 ratio, and a wedge at 30° of incidence. The model has 370 mm in length and 36 mm in thickness.

Inside the flat plate, a 2D teledriven-gear frame (10 cm x 15 cm) supports the optical head of the LV, the optical fibre and a mirror. The laser beams are focused in the measuring volume through the circular mirror and the wall of the plate equipped with an optical quality glass. As sketched in Figure 2b, the measurement volume can be displaced along a direction y perpendicular to the wall (on 25 mm with a precision of 0.1 µm). The x-displacement along the chord is about 200mm.

The front lens of the optical head has 50 mm in focal length and the beams spacing is 8 mm. The interfringe is 3.2 µm and the ellipsoïdal volume containing the interference fringes has for physical size : x = 0.3 mm ; y = 1.2 mm ; z = 0.12 mm ; where xoy is the plane normal to the wall as shown in Fig. 2b. Although the longest dimension (y = 1.2 mm) is along the normal to the wall, the operating mode of the counting system provides a significant reduction of the spatial resolution along y. The data validations are indeed performed by comparison of velocity measurements over 5 and 8 consecutive fringes (relative error test less than 2/1000), so that the regions located near the ellipsoidal shape ends do not contributed to the measure. In the xoy plane, the effective measuring section is thus nearly rhomboidal and its length axis (xe, ye) are : 0.15 mm ≤ xe ≤ 0.20 mm and 0.40 mm ≤ ye ≤ 0.60 mm.

It can be noticed that the reduced size of the effective measuring volume does not eliminate the interference reflexion problem on the wall glass for distances very close to the wall (y < 0.40 mm). Moreover, the alternative of mounting the optical head and its associated 2D displacement device in a different arrangement (for instance in order to exchange the xe and ye axis) will be improved in a future work.

The LV system operates in the back-scatter mode and the data acquisition is made on APPLE Mac IIX from a DANTEC counter through an IEEE 488 interface. The software used for steady and unsteady data management is from NATIONAL INSTRUMENTS (Labview system). Figure 3 presents the laser source, the optical head mounted in the flat plate and connected to the laser by a fibre, and the block diagram of data acquisition.

It should be noticed that one of the main advantage in using the optical fibre system is to overcome some practical problems generally raised with classical LV systems (misalignements, long focal distances, mirror displacements, ...). Moreover, in the optical fibre option the sub-systems of signal emission and reception can be set in a fixed position and far from the measuring zone as scketched in Fig. 3, where the beam sliptter, the bragg cell, the photomultiplier as well as the Laser source are located at about 2 meters from the test section.

Concerning the seeding of the flow different kinds of particles have been tested including D.O.P, oil mixture and incense particles. The optimisation in seeding the flow has been obtained as a function of both the size of injected particles and the position of the injection zone as illustrated in Fig. 4. A little tank located at the leading-edge of the flat plate allows the seeding of the flow, directly from the wall into the boundary-layer. It is also possible to seed the flow by means of a streamlined tube located either 2 chords upstream of the model, or inside the suction chamber located upstream of the test section (see Fig. 4). The best rates of data validation have been obtained using a mixture of alcohol (80 %) and glycerine (20 %). This mixture provides a validation data rate of 500 KHz with validation on 5 and 8 fringes about 80-90%. The mean diameter of the particles is 2×10^{-6} m.

III. Statistical Data Reduction Procedure

The data acquisition and reduction technique are made using an ensemble average method suited for periodic unsteady flow investigations[22,23]. Data acquisitions are performed by means of a DANTEC counter (55L90) associated with an interface (DANTEC 57G20) and a Macintosh computer (Mac IIX) operating under the Labview system (see Fig. 3).

Due to the periodicity of the flow, each period is considered as a specific sample of the same phenomenon, so that the velocity u(t) can be obtained at each phase angle ωt as the averaged value of the velocity samples recorded at the same

given phase angle and over a large number of cycles, according to the following statistical procedure (see Fig. 5) :

For each particle validated by the counter the velocity u and the time t along the period T of the plate motion are provided by the acquisition system. The total number N_S of velocity samples Un(j), recorded at different cycles of oscillation n(j) and at different instants tj over the cycles, is arbitrarily fixed (usually $5000<N_S<6000$ with the buffer memory used in the present test), and constitutes a matrix $U_{n(j)}(t_j)$ defined as :

$$U_{n(j)}(t_j) = \begin{array}{c} \begin{matrix} t_0 & t_1 & \cdots & t_j & \cdots & t_0+T \end{matrix} \\ \begin{bmatrix} u_{1(0)} & u_{1(1)} & \cdots & u_{1(j)} & \cdots & u_{1(0+T)} \\ u_{2(0)} & u_{2(1)} & \cdots & u_{2(j)} & \cdots & u_{2(0+T)} \\ | & | & | & | & | & | \\ u_{i(0)} & u_{i(1)} & \cdots & u_{i(j)} & \cdots & u_{i(0+T)} \\ | & | & | & | & | & | \\ u_{n(0)} & u_{n(1)} & \cdots & u_{n(j)} & \cdots & u_{n(0+T)} \end{bmatrix} \end{array}$$

Due to the random character of both the seeding and the counter validation and because the number N_S is fixed "a priori" , it must be noticed that a different number of data are recorded at the different instants of the period (e.g. n is a funtion of tj). From this data matrix, the instantaneous velocity u(t) is splitted in the form :

$$u(t) = \bar{u} + \tilde{u}(t) + u'(t) \qquad (1)$$

where : $\bar{u} = \frac{1}{T}\int_0^T u(t)\,dt$ is the mean velocity (averaged in time);

$\tilde{u}(t) = \sum_{n=1}^{N} \Delta U_n \cos(n\omega t + \phi_n)$ is the periodic velocity component and u' is the random fluctuation ($\overline{u'} = 0$).

From the previous triple decomposition, the quantity $< u > = \bar{u} + \tilde{u}(t)$ is obtained by a phase average procedure. That means that $< u >$ represents the ensemble average of velocity samples recorded along different cycles n(j) but at the same instant tj:

$$< u > = \bar{u} + \tilde{u}(t_j) = \frac{1}{n(j)} \sum_{n=1}^{n(j)} u_i(t_j) \qquad (2)$$

wich can be also written

$$< u > = \bar{u} + \sum_{n=1}^{N} \Delta U_n \cos(n\omega t + \phi_n) \qquad (3)$$

where $\bar{u}$, Δu_n and Φ_n are deduced from a Fast Fourier Transform algorithm. Thus, Δu_n represents the amplitudes of the nth harmonic components of the velocity fluctuations in the boundary-layer. Φ_n are the respective phase angles of these components.

However, in the previous equations (1)-(3), the assumption is made that for each cycle n(j) the velocities $u_{n(j)}(t_j)$ are recorded at the same instant tj. Obviously, all these velocity samples cannot pratically be recorded at the same instant of the period, and a simultaneous criterion of measurement between each cycle is defined as (see Figure 5):

$t_j = T_j$ if $(T_j - \Delta t/2) \leq t_j \leq (T_j + \Delta t/2)$ (4)

In the present tests the phase interval has been selected at $\Delta(\omega t) = 4°$, so that the time interval of simultaneousness is $\Delta t \approx T/100$. Finally, the RMS value of the velocity fluctuation $u' = u - < u >$ is deduced from the previous expressions, as :

$$\left[\overline{u'^2(t)}\right]^{1/2} = \left[\frac{1}{n(j)} \sum_{n=1}^{n(j)} u'^2(t)\right]^{1/2} \qquad (5)$$

IV. Steady Flow Results

In order to check both the particles seeding procedure and the capability of the LV embodied technique, several preliminary tests have been performed in the steady configuration around the flat plate at rest in the uniform flow.

Fig. 6 gives an example of the velocity profile measured in the flat plate boundary-layer when particles are seeded from the leading-edge wall of the model for the following steady conditions : x/c = 0.23 ; $U_\infty = 11.4\ ms^{-1}$ and $\alpha_0 = 0°$.

Evidence of the influence of this type of seeding procedure is given in the Figure, when comparing the LV-optical fibre results to those provided either by the classical hot-wire technique (with and without injection of particles) or by the theoretical laminar and turbulent velocity profiles[7,8]. From the results in Fig. 6, it can be also noticed that the distorsion of the flow due to the seeding mode from the model leading-edge is equally captured by the LV and the hot-wire measurements. In this case the transtion to turbulence is generated by the particles injection within the boundary-layer itself.

Similar flow perturbations and boundary-layer transitional effects have been also exhibited[20] when the seeding of the flow is realized by means of a streamlined tube located two chords upstream of the plate. On the other hand, when the particles injection is realized from upstream of the wind tunnel test section, the LV and HW measurements are shown in good agreement as illustrated in Fig. 7. The results indicate that both experimental profiles also match the theoretical profile deduced from the Blasius flow solution. Consequently, the particles seeding mode from the suction chamber of

the wind tunnel has been used for all the steady and unsteady tests presented in this study.

In steady flow, when the model is at rest in the uniform flow, the efficiency of the present LV-optical fibre technique is clearly demonstrated in Fig 8-10 for three different distances from the leading-edge x/c = 0.23 ; 0.39 ; 0.59 and two external velocities U_∞ = 8.34 ms^{-1} ; 16.61 ms^{-1} at the incidence α_0 =0° of the flat plate. The dimensionless distance from the wall $y.[R_{ex}/x]^{1/2}$ is plotted versus the boundary-layer velocity profile u/U_e and compared to the theorical results deduced from the laminar Blasius flow solution and the 1/7 law for the turbulent flow. LV measurements and calculation results are shown to be in good agreement and indicate the occurrence of the transition to the turbulent boundary-layer regime at a distance x/c > 0.40 and for the highest value at the external velocity U_e = 16.61 ms^{-1}.

The influence of α_0 on the boundary-layer development is exemplified in Fig. 11 where the velocity profiles have been measured at the fixed absisse x/c = 0.23 and for angle-of-attacks varying from 0° to 4°. As soon as $\alpha_0 \geq 3°$ the results in Fig. 11 indicated that the transition to turbulence is detected near the leading-edge.

From the steady results shown in Figures 6 to 11, it can be also noticed that the present LV-Optical fibre method becomes inadequate for distances normal to the wall less than 4/10 mm. As previously discussed, this is mainly due to the dimension of the effective measuring volume along the y-direction, associated to the back-scatter mode used in the present tests. The measurement distance normal to the wall could be reduced by improving the optical quality of the glass window mounted flush on the surface and by integrating an appropriate optical head and beam expansion device to the LV system. In the same way, a different geometrical arrangement of the optical head and its associated displacement device could also improve the measuring technique performance. However, all these points of improvements are beyond the scope of the present study which is focused on testing the capability of the LV technique in nonsteady flow.

V. Unsteady Flow Results

Using the data acquisition and reduction technique previously described, the velocity profile through the unsteady boundary-layer has been performed at three longitudinal distances x/c along the plate and at different set of oscillating parameters of the fore-and-aft motion, e.g. α_0, λ, k.

As an example, Figures 12-14 present the recorded velocity waveforms $u/U_e = u/U_e(\omega t)$ at several distances y from the wall. Figures 12, 13 concern the abscissa x/c = 0.23 at α_0 = 0 ° and two values of the oscillating parameters (λ= 0.09 ; k = 0.30). While Fig. 14 concerns the case x/c = 0.39 ; α_0 = 0° ; λ = 0.29 ; k = 0.30.

In each case, the boundary-layer survey has been realized at 21 different values of y. Only five of them are plotted in Figures 12-14 for y varying from y = 0.625 mm to y = 5 mm. When using the phase average technique the period is divided in 32 equal parts and the acquisition is made until 5120 data are validated and recorded over the period. In such a way, each of the 32 data points constituting the time-dependent velocity profile is deducted from an histogram constructed over more than 100 samples recorded at a given phase ωt of the period.

The results in Figures 12-14 clearly indicate that outside the boundary-layer, the velocity profile is varying sinusoidally with no phase shift (see for instance the profile at y = 4 mm in Figures 12, 13 and at y = 5 mm in Figure 14). When decreasing y and entering the boundary-layer, the amplitude of velocity fluctuations decreases and the profile presents a phase shift with the potential flow as it is the case in oscillatory flow around the model at rest[6,7].

From these time-dependent velocity waveforms $u/U_e = u/U_e(\omega t)$, the evolution of the harmonic components of the velocity through the boundary-layer is then obtained in the form of equation (3). Figure 15a, b, c gives the evolution of the mean component $\overline{u}/U_e$ and of the first harmonic components ($\Delta u_1/\Delta U_e$; Φ) at the following parameters : x/c = 0.23 ; α_0 =0° ; λ = 0.29 ; k = 0.30. The results show that the unsteady mean profile $\overline{u}/U_e$ is very close to the corresponding steady behaviour (Figure 15a). The amplitude $\Delta u_1/\Delta U_e$ is increased in the outer part of the boundary layer and attenuated near the wall due to the predominance of viscous effect (Figure 15b). Also shown in Figure 15c is the increase of the phase shift Φ when the distance to the wall is decreased. All these unsteady laminar boundary-layer features well corroborate those previously obtained in the oscillatory flow around the flat plate at rest (see for exemple refs. 4,5,14).

The influence of the oscillating parameter λ on the evolution of the three first harmonic components of the boundary-layer velocity is given in Figure 16a, b, c, for the laminar regime at x/c = 0.23 and α_0 = 0°. The mean velocity component $\overline{u}/U_e$ is shown to be slightly modified by the variation of λ (Figure 16a). The amplitude of the velocity fluctuations $\Delta u_1/\Delta U_e$ are increased in the region $2 \leq \eta \leq 5$ and attenuated near the wall for $\eta \leq 2$ (Fig. 16b). Also shown in Fig 16c is the increase in the phase shift Φ as the amplitude of the external velocity oscillation λ increases.

In order to check more completely the efficiency of the LV embodied technique, the present unsteady boundary-layer measurements have been also compared to some existing experimental and analytical results obtained around the model placed at rest in the oscillatory flow.

Figures 17 and 18 give the comparison between the present LV measurements with hot-wire measurements [14] and laminar calculation results [7] obtained on a flat plate set at zero incidence in the pulsated flow for similar values of the oscillating parameters $\overline{X}$ and λ . It can be noticed that the calculations results and the LV measuremeents are performed at exactly the same sets of parameters ($\overline{X} = 0.10$, $\lambda = 0.19$) in Fig 17, and ($\overline{X} = 0.14$, $\lambda = 0.29$) in Fig. 18. These two sets of parameters are close but not exactly the same for the experimental data obtained in reference 14 using the hot-wire technique.

Nevertheless, for these low and moderate values of the oscillating parameters $\overline{X}$ and λ, the results in Figures 17 and 18 concerning the amplitude of velocity fluctuations $\Delta u1/\Delta U_e$ indicate a good agreement between LV-measurements, HW-measurements and calculation results. A similar good agreement between LV-measurements and the calculation results deduced from the lighthill approximation is also shown in Figures 19 and 20 concerning the phase Φ of the boundary-layer velocity. In this case the hot-wire experiments are not available in reference 14 and the comparison only concerns the LV-measurements and the calculation results obtained at the same values of the $\overline{X}$ and λ parameters.

The previous comparisons also confirm that equivalent unsteady boundary-layer characteristics are obtained either when oscillating the flat plate in the uniform freestream, or when oscillating the flow around the plate at rest, at least for the low or moderated parameters $\overline{X}$, λ, α_0 of the laminar boundary-layer regime considered in the present tests.

VI. Conclusion

A new velocity measurement technique using an embodied LV-optical fibre system has been developped and tested in determining the boundary-layer velocity profiles on a flat plate oscillating in fore-and-aft motion.

From the present first set of results it has been shown that this LV technique appears to be a powerful tool for nonsteady measurements near a moving wall.

The efficiency of the measurement method has been established by comparison with classical hot-wire measurements and theoretical results obtained in the reciprocal flow configuration of a model placed at rest in an oscillatory flow. The comparisons have been limited to laminar boundary layer regimes and low or moderate oscillating parameters $\overline{X}$, λ, α_0 and k.

Although the range of oscillating parameters remains limited, these results obtained in a moving frame by means of a non-intrusive LV technique constitute one of the first set of data that clearly corroborates the reprocity principle and the equivalence of the flowfields generated either by oscillating the body in the freestream, or by oscillating the flow around the body at rest.

In the future, the efficiency of the LV embodied technique will be checked more extensively by studying higher values of the oscillating parameters of the plate, transition, turbulent and separation regimes. As previously mentioned developments of this LV technique, in order to reduce the measurement distance to the wall, as well as the spatial resolution along the y-direction, will be also undertaken in future works.

References

[1]Mc Croskey, W.J., "The phenomenon of dynamic stall.", NASA TM.-81264, 1981.

[2]Mc Croskey, W.J. and Pucci, S.L., "Viscous-inviscid interaction on oscillating airfoils in subsonic flows.", *A.I.A.A. Journal*, Vol. 20, 1982, pp. 167-174.

[3]Telionis, D.P. and Tsahalis, D.T., "Unsteady laminar separation over cylinder started impulsively from rest.", *Acta Astronautica*, Vol. 1, 1974.

[4]Telionis, D.P., "Unsteady viscous flow.", Springer Verlag Editor, N.Y., 1981.

[5]Cebeci, T., Carr, L.W., Khattab, A.A. and Schimke, S.M., "Computational aspects of unsteady flows.", AGARD CP836, Göttingen, 1985.

[6]Cousteix, J. and Houdeville, R., "Couches limites instationnaires.", , ONERA/CERT Technical Report OA 53-2259, 1983.

[7]Schlichting, H., "Boundary layer theory.", Mc Graw-Hill Book Company, Inc., N.Y., 1954.

[8]Lighthill, M.J., "The response of laminar skin friction and heat transfert to fluctuations in the stream velocity.", *Proceedings of Royal Society*, Vol. 224, Serie A, 1954.

[9]Cousteix, J., Le Balleur, J.C. and Houdeville, R., "Calcul de couches limites instationnaires en mode direct ou inverse.", *La Recherche Aérospatiale*, N° 3, 1980, pp. 147-157.

[10]Samroth, S.J., "A Navier Stokes calculation of the airfoil dynamic stall process.", Workshop on unsteady separated flows, Francis and Luttges Editors, Colorado Springs, 1984.

[11]Cebeci, T., "Unsteady boundary layers with an intelligent numerical scheme.", *Journal of Fluid Mechanics*, Vol. 163, 1986.

[12]Cousteix, J., "Three dimensional and unsteady boundary layers computations.", *Annual Review of Fluid Mechanics*, Vol. 18, 1986.

[13]Bellhouse, B.J. and Schultz, D.L., "Determination of mean and dynamic skin friction, separation and transition in low-speed flow with heated element.", *Journal of Fluid Mechanics*, Vol. 24, 1966, pp. 379-400.

[14]Hill, P.G. and Stenning, A.H., "Laminar boundary layers in oscillatory flow.", Transactions of A.S.M.E., *Journal of Basic Engineering*, Vol. 82, 1968, pp. 593-608.

[15]Despard, R.A. and Miller, J.A., "Separation in oscillating laminar boundary layer flows.", *Journal of Fluid Mechanics*, Vol. 47, part 1, 1971, pp. 21-31.

[16]Mc Croskey, W.J. and Durbin, E.J., "Flow angle and shear stress measurements using heated films and wires.", Transactions of A.S.M.E., *Journal of Basic Engineering*, Vol. 94, Serie D, N° 1, 1972, pp. 46-52.

[17]Binder, G., Tardu, S., Blackwelder R.and Kueny, J.L., "Etude expérimentale de couches limites instationnaires soumises à des gradients de pression moyens, nuls et positifs.", AGARD CP386, 1985.

[18]Maresca, C., Favier, D. and Rebont, J., "Unsteady aerodynamics of an airfoil at hight angle of attack performing linear oscillations in an uniform stream.", *Journal of the American Helicopter Society*, Vol. 26, 1981, pp. 40-45.

[19]Favier, D., Agnes, A., Barbi, C. and Maresca, C., "Combined translation/pitch motion : a new airfoil dynamic stall simulation.", *Journal of Aircraft*, Vol. 25, N° 9, , 1988, pp. 805-814.

[20]Favier, D., Maresca, C., Belleudy, J. and Renon, P., "Etude expérimentale de la couche limite instationnaire sur une plaque plane oscillante.", Convention DRET 87/272, Janvier 1990.

[21]Schachenmann, A. and Tropea, C., "LTV signal processing in turbulent flows.", *Proceedings of the Use of Computers in Laser Anemometry*, ISL, Saint-Louis, May 1987.

[22]Bonnet, J.L. and Houdeville, R., "Mesures par vélocimetrie Laser de la couche limite sur une plaque plane en oscillation autour d'une incidence moyenne.", ONERA/CERT Technical Report, RT 18/501411, April 1988.

[23]Cousteix, J. and Houdeville, R., "Effects of unsteadiness on turbulent boundary layers.", *Fluid Dynamics Lecture Series of V.K.I.*, July 1988.

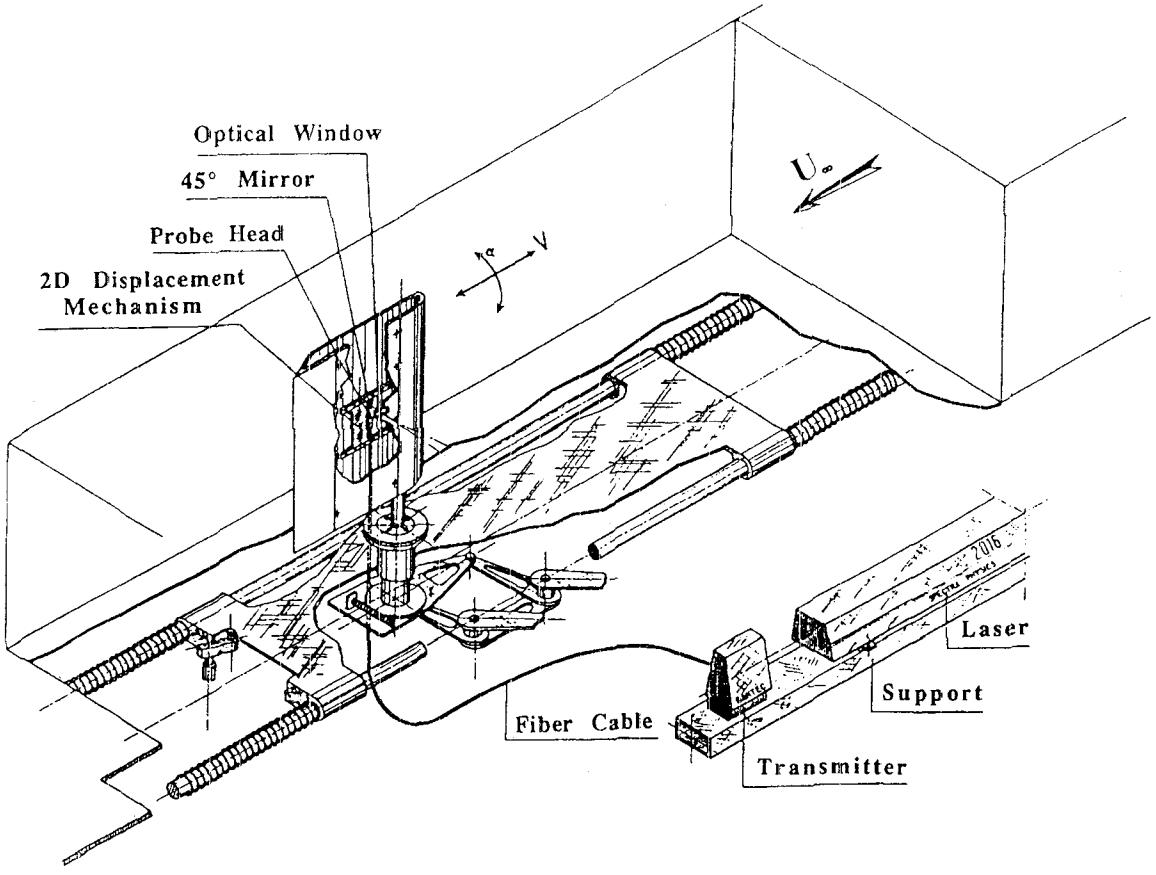

Fig. 1 Experimental set up and embodied LV-optical fibre.

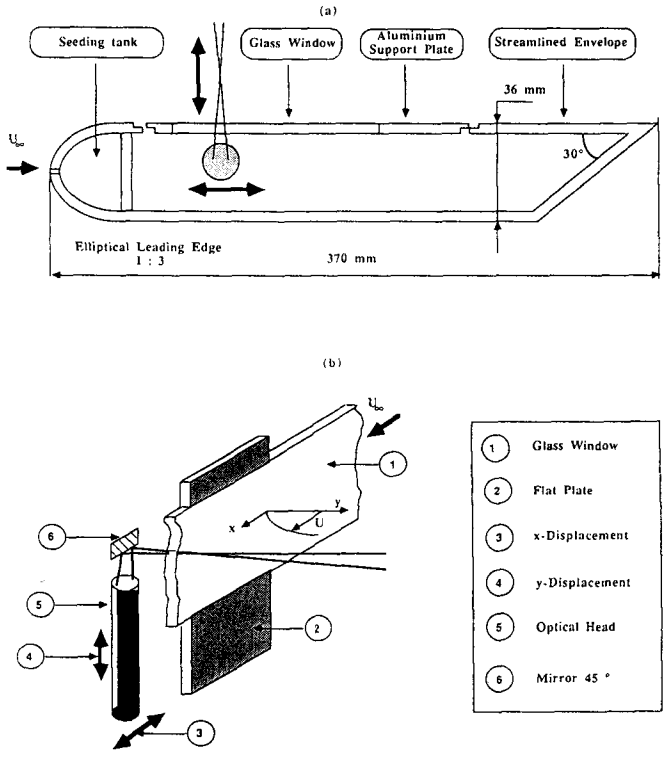

Fig. 2 Instrumented model : a) flat plate geometry; b) optical head mounting system.

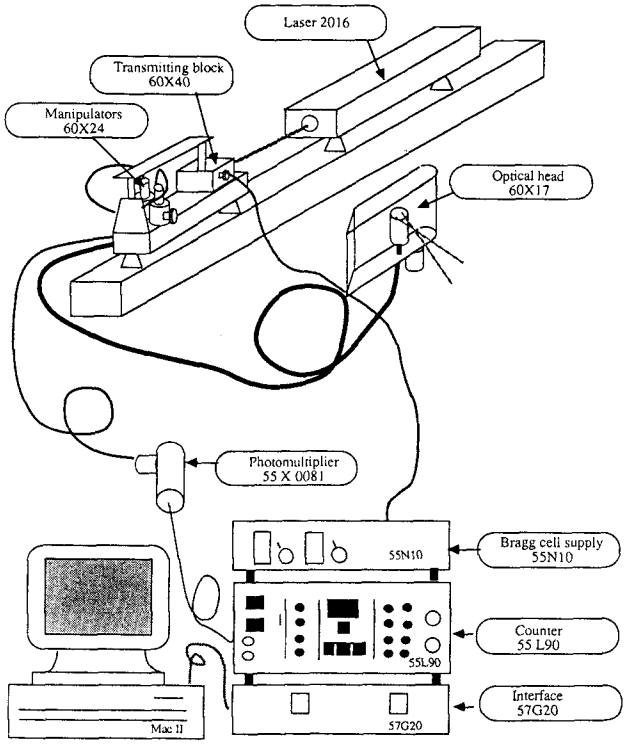

Fig.3 Block diagram of LV system and data acquisition.

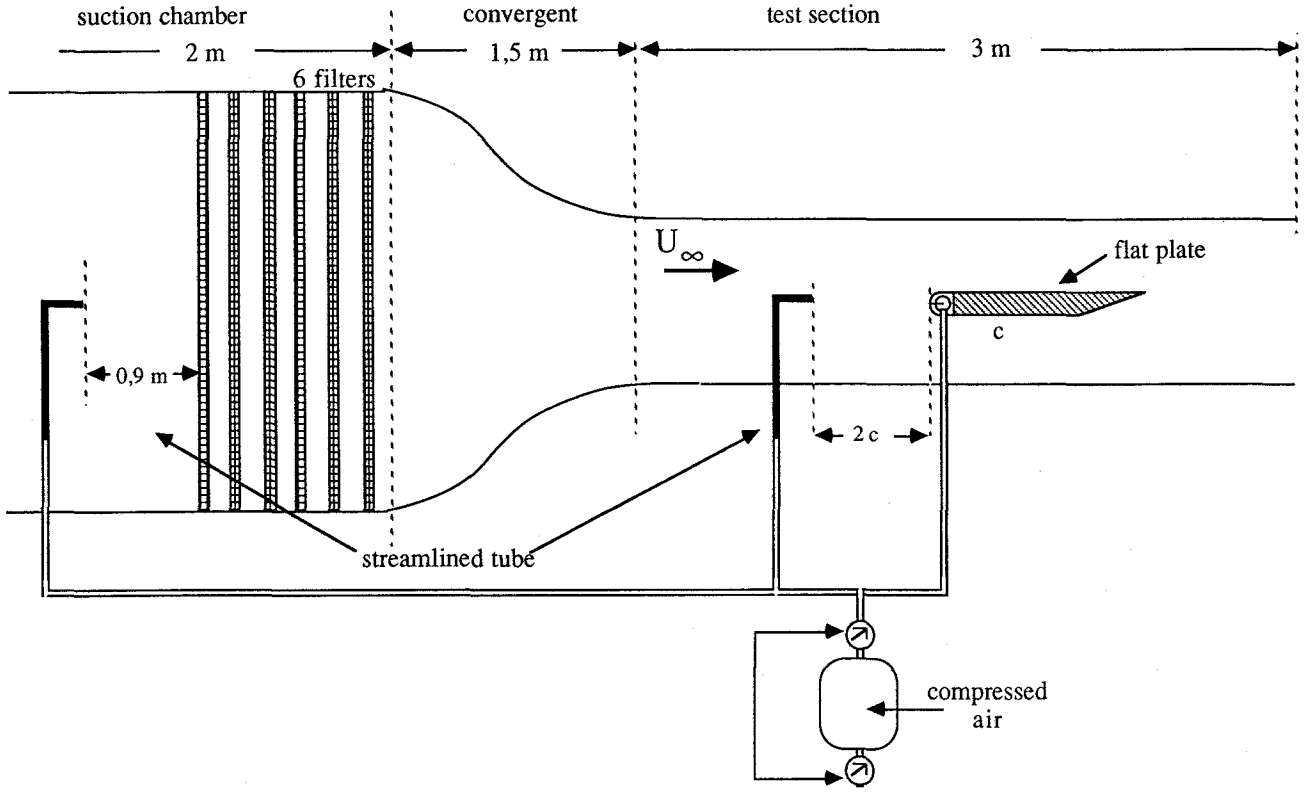

Fig. 4 Seeding of the flow : zones of particles injection.

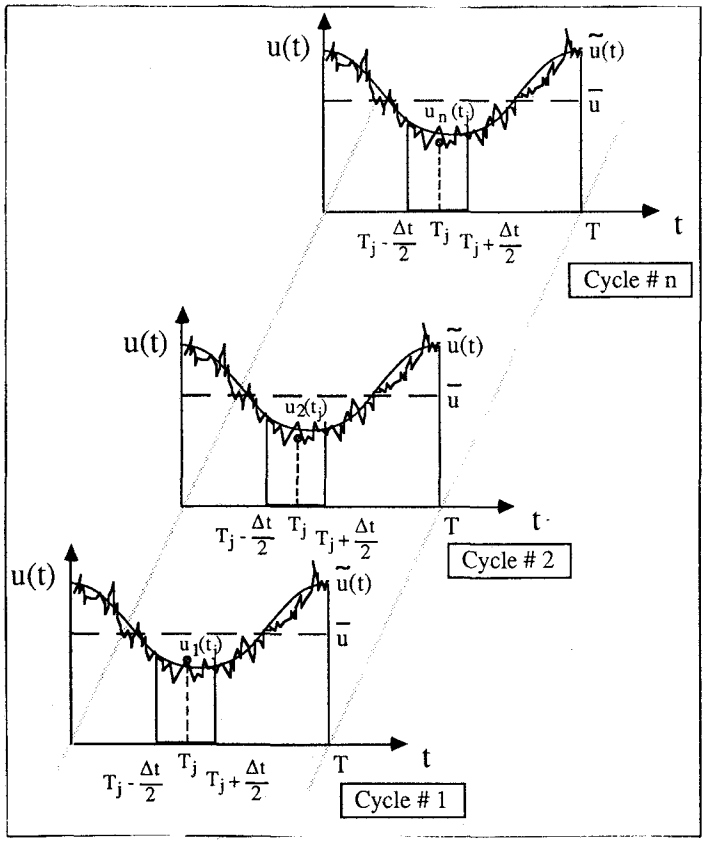

- Instantaneous velocity

$$u = \bar{u} + \tilde{u}(t) + u'(t)$$

- Mean velocity (time average)

$$\bar{u} = \frac{1}{T}\int_0^T u(t)\,dt$$

- Periodic component

$$\tilde{u}(t) = \sum_{n=1}^{N} \Delta u_n \cos(n\omega t + \phi_n)$$

- Ensemble average velocity

$$\langle u \rangle = \bar{u} + \tilde{u}(t_j) = \frac{1}{n(j)} \sum_{i=1}^{n(j)} u_i(t_j)$$

- R.M.S. fluctuations

$$u'(t) = u - \langle u \rangle$$

$$\left[\overline{u'^2}(t)\right]^{\frac{1}{2}} = \left[\frac{1}{n(j)} \sum_{n=1}^{n(j)} u'^2(t)\right]^{\frac{1}{2}}$$

- Simultaneousness criteria

$$\text{If} \quad T_j - \frac{\Delta t}{2} \le t_j \le T_j + \frac{\Delta t}{2} \qquad t_j = T_j$$

$$\text{with :} \quad \Delta(\omega t) = 4° \; ; \quad \Delta t \approx T/100$$

Fig. 5 Statistical data reduction.

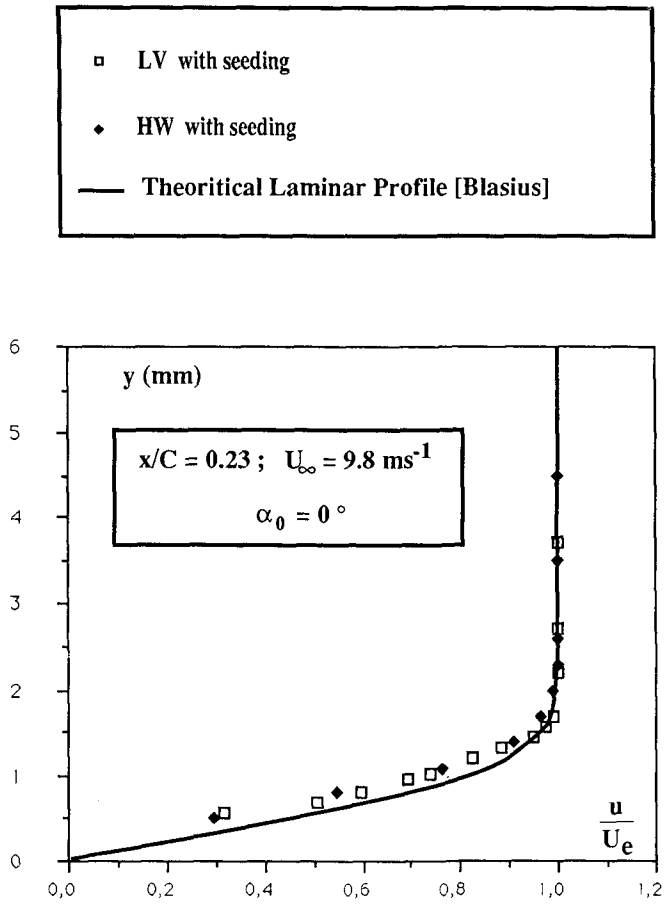

Fig. 7 Seeding from the suction chamber.

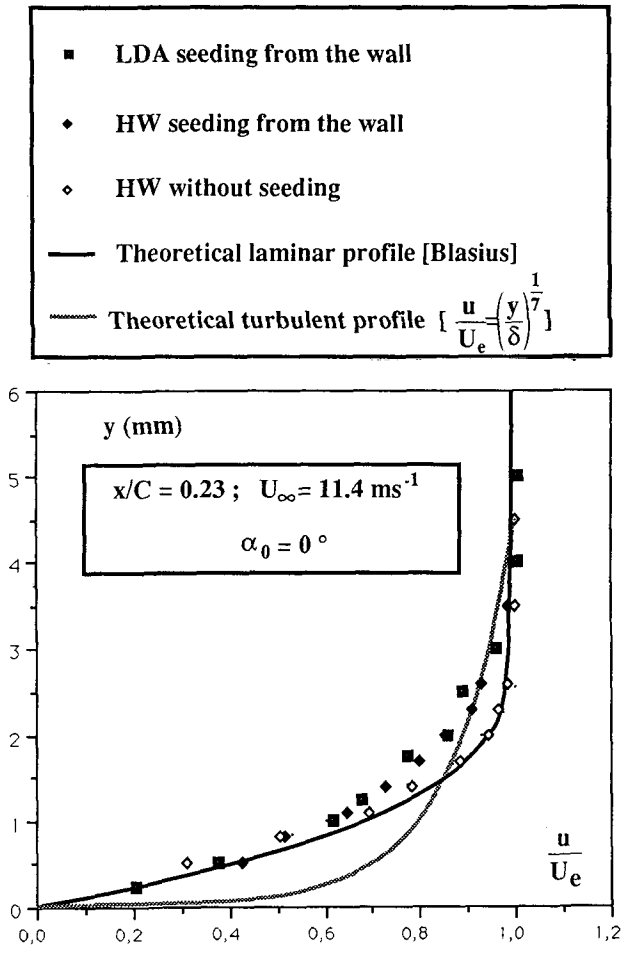

Fig. 6 Influence of the seeding from the wall.

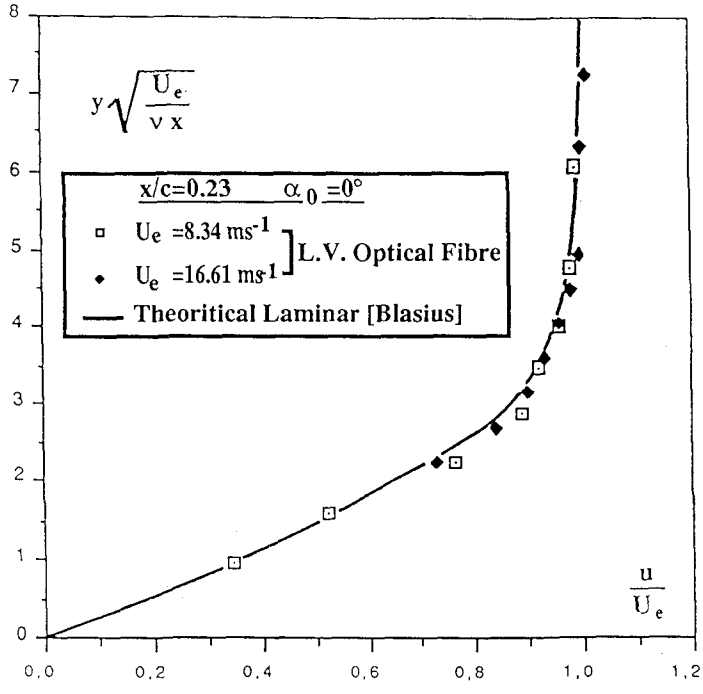

Fig. 8 Comparison calculation/experiment in steady flow at $\alpha_0 = 0°$; x/c = 0.23.

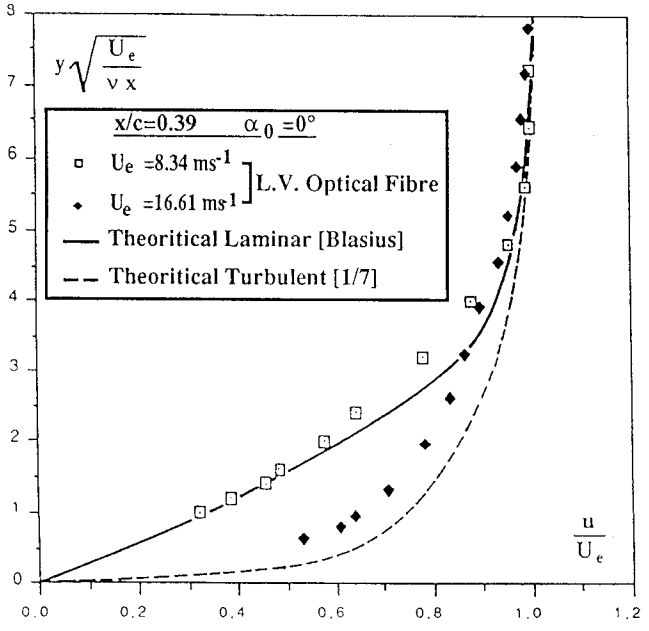

Fig. 9 Comparison calculation/experiment in steady flow at α_0 = 0°; x/c = 0.39.

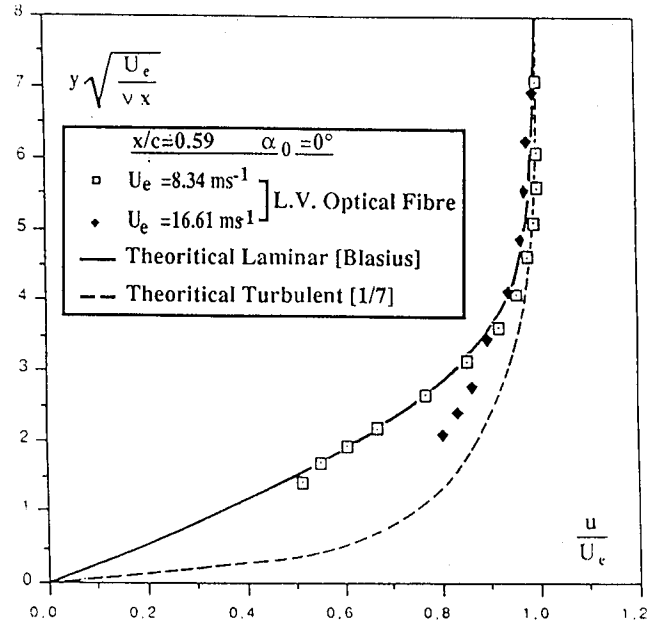

Fig. 10 Comparison calculation/experiment in steady flow at α_0 = 0°; x/c = 0.59.

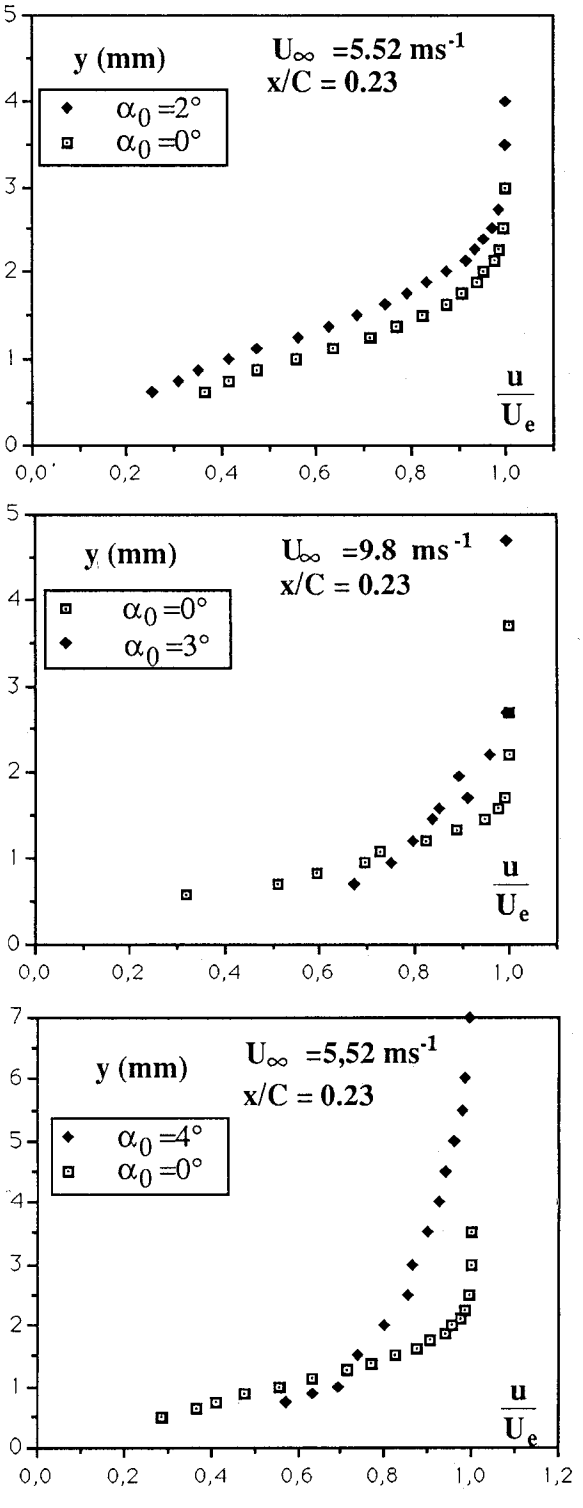

Fig. 11 Influence of α_0 on the upper side velocity profile at x/c = 0.23.

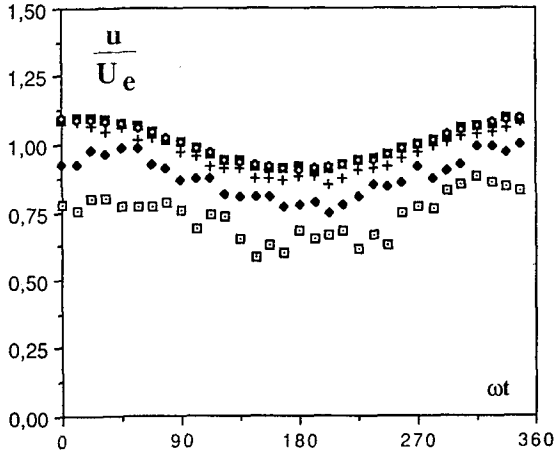

Fig. 12 Velocity waveforms at different distances y from the wall : x/c = 0.23 ; α_0 = 0° ; λ = 0.09 ; k = 0.10.

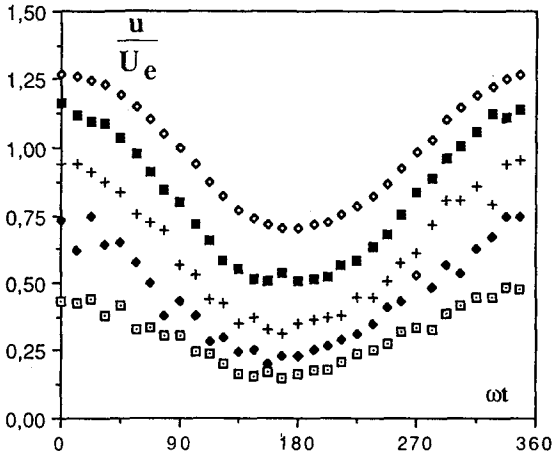

Fig. 13 Velocity waveforms at different distances y from the wall : x/c = 0.23 ; α_0 = 0° ; λ = 0.29 ; k = 0.30.

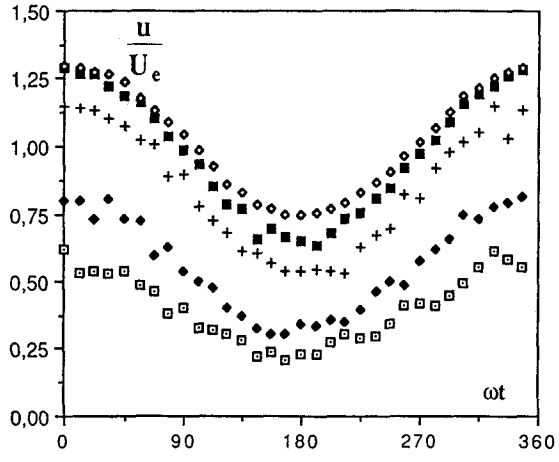

Fig. 14 Velocity waveforms at different distances y from the wall : x/c = 0.39 ; α_0 = 0° ; λ = 0.29 ; k = 0.30.

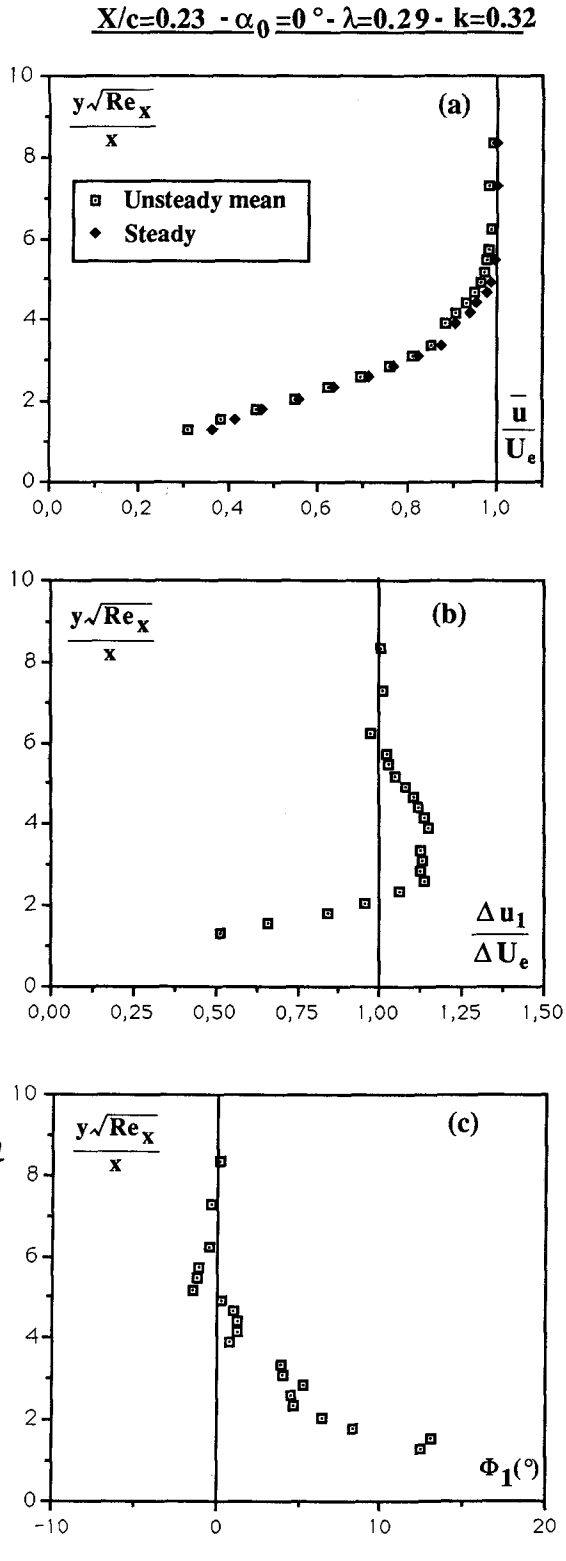

Fig. 15 Harmonic components of the velocity : a) mean value ; b) amplitude fluctuations ; c) phase shift.

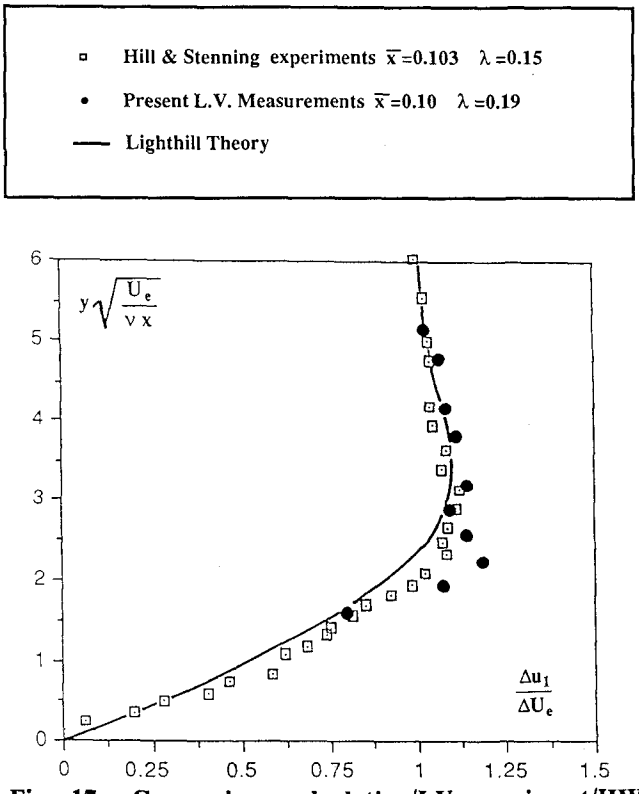

Fig. 17 Comparison calculation/LV-experiment/HW-experiment on the amplitude of velocity fluctuations at $\overline{X}$ = 0.10.

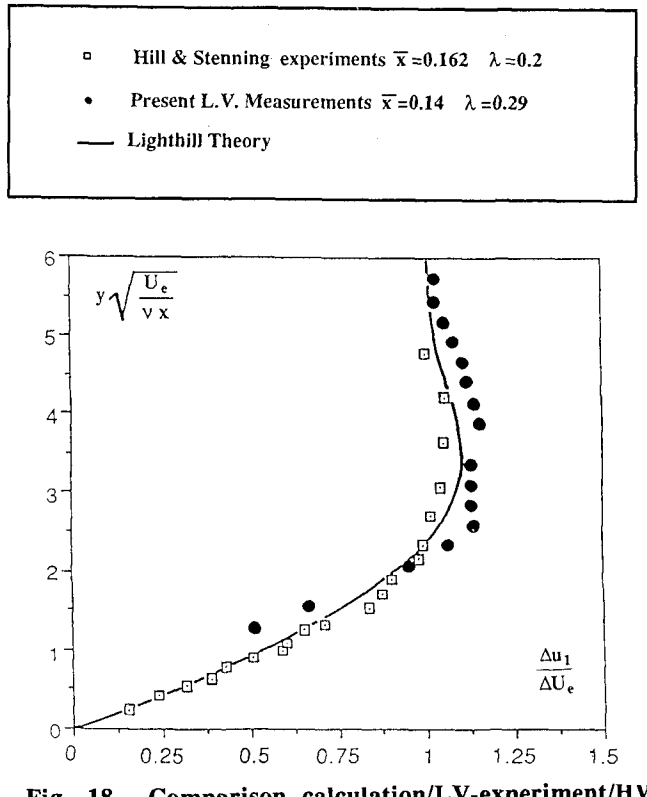

Fig. 18 Comparison calculation/LV-experiment/HW-experiment on the amplitude of velocity fluctuations at $\overline{X}$ = 0.14.

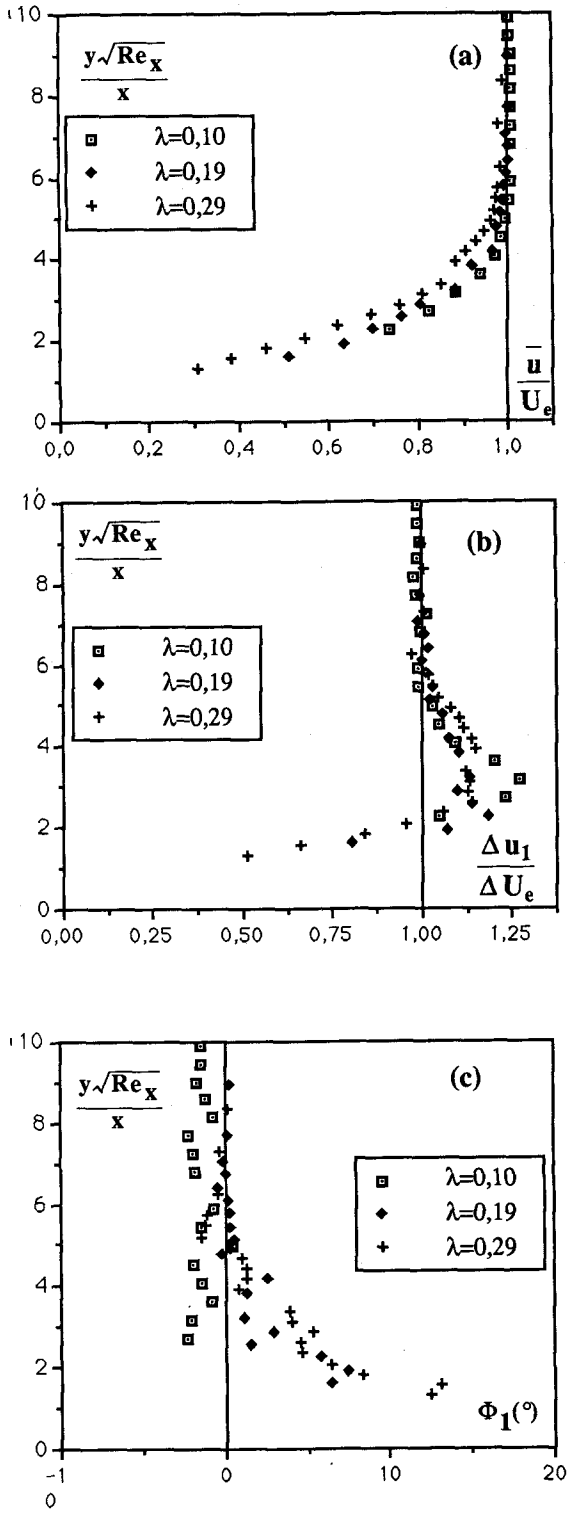

Fig. 16 Influence of λ on the harmonic components.

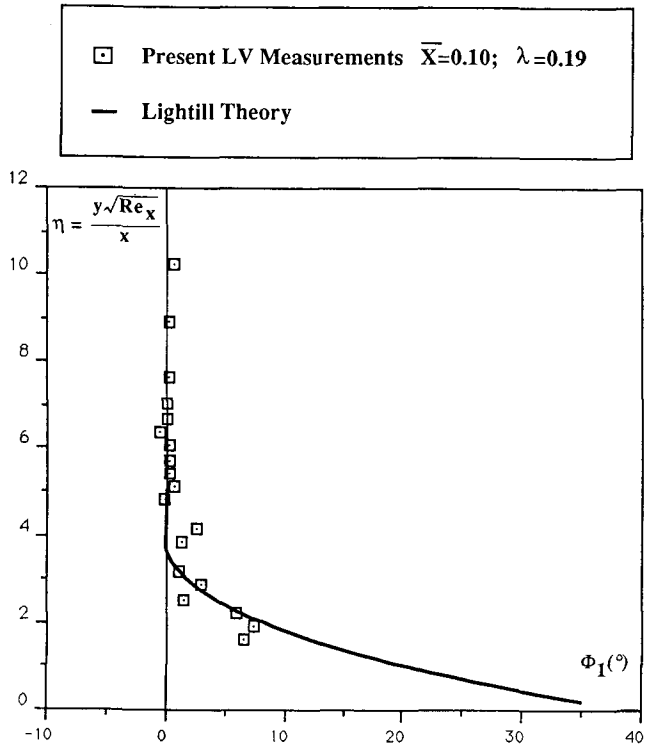

Fig. 19 Comparison calculation/LV-experiment on the phase shift at $\overline{X}$ = 0.10.

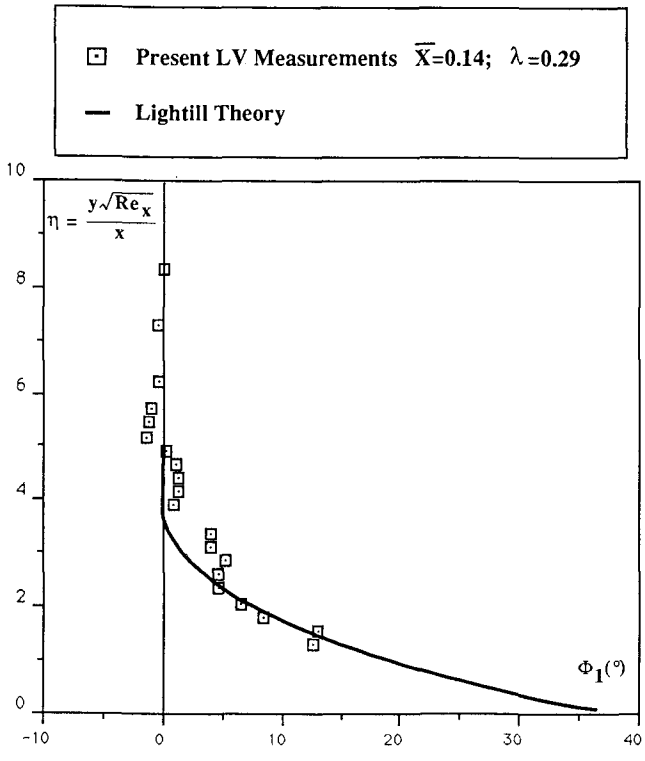

Fig. 20 Comparison calculation/LV-experiment on the phase shift at $\overline{X}$ = 0.14.